Journal of Hydrology 553 (2017) 408–418

Contents lists available at ScienceDirect

Journal of Hydrology

journal homepage: www.elsevier.com/locate/jhydrol

Research papers

Using radiative signatures to diagnose the cause of warming during the 2013–2014 Californian drought

Sebastian Wolf [a,*], Dongqin Yin [b,c], Michael L. Roderick [b,c]

[a] Department of Environmental Systems Science, ETH Zurich, 8092 Zurich, Switzerland
[b] Research School of Earth Sciences, Australian National University, Canberra, Australia
[c] Australian Research Council Centre of Excellence for Climate System Science, Canberra, Australia

ARTICLE INFO

Article history:
Received 18 November 2016
Received in revised form 7 July 2017
Accepted 10 July 2017
Available online 11 July 2017
This manuscript was handled by Tim R. McVicar, Editor-in-Chief, with the assistance of Sergio M. Vicente-Serrano, Associate Editor

Keywords:
California
Drought
Land-surface feedbacks
Radiative signature
Anthropogenic warming
Greenhouse effect

ABSTRACT

California recently experienced among the worst droughts of the last century, with exceptional precipitation deficits and co-occurring record high temperatures. The dry conditions caused severe water shortages in one of the economically most important agricultural regions of the US. It has recently been hypothesized that anthropogenic warming is increasing the likelihood of such extreme droughts in California, or more specifically, that warmer temperatures from the enhanced greenhouse effect intensify drought conditions. However, separating the cause and effect is difficult because the dry conditions lead to a reduction in evaporative cooling that contributes to the warming. Here we investigate and compare the forcing of long-term greenhouse-induced warming with the short-term warming during the 2013–2014 Californian drought. We use the concept of radiative signatures to investigate the source of the radiative perturbation during the drought, relate the signatures to expected changes due to anthropogenic warming, and assess the cause of warming based on observed changes in the surface energy balance compared to the period 2001–2012. We found that the recent meteorological drought based on precipitation deficits was characterised by an increase in incoming shortwave radiation coupled with a decline in incoming longwave radiation, which contributed to record warm temperatures. In contrast, climate models project that anthropogenic warming is accompanied by little change in incoming shortwave but a large increase in incoming longwave radiation. The warming during the drought was associated with increased incoming shortwave radiation in combination with reduced evaporative cooling from water deficits, which enhanced surface temperatures and sensible heat transfer to the atmosphere. Our analyses demonstrate that radiative signatures are a powerful tool to differentiate the source of perturbations in the surface energy balance at monthly to seasonal time scales.

1. Introduction

The state of California experienced severe drought conditions during 2013–2014 that were exceptional during the last century (Diaz and Wahl, 2015; Mann and Gleick, 2015; Seager et al., 2015) and paleoclimate reconstructions suggest that it was among the most severe droughts of the last millennium (Griffin and Anchukaitis, 2014). The water year (Oct–Sep) 2013 was the 24th driest year on record since 1896 with precipitation totals of 431 mm yr^{-1}, or −23% below the long-term mean of 1896–2014 (562 mm yr^{-1}) (NOAA, 2016). The following water year 2014 was the 3rd driest with precipitation totals of 315 mm yr^{-1}, or −44% below average, and the year was also among the warmest on record (NOAA, 2016). The persisting multi-year drought caused severe water shortages in one of the economically most important agricultural regions of the US and prompted unprecedented statewide water restrictions during the drought (AghaKouchak et al., 2015; Cooley et al., 2015; Howitt et al., 2014).

There is intense socio-economic and scientific interest in all aspects of the Californian drought. In terms of the underlying 'cause', the research to date has focussed on two broad themes. The first theme analyses the changes in circulation patterns that are associated with the low precipitation since 2012 (Seager et al., 2015; Swain et al., 2016, 2014; Wang et al., 2014). The focus is to understand the large-scale atmospheric dynamics that are associated with the low rainfall totals. In essence, this approach examines the changes in water supply from synoptic-scale atmospheric transport. The second theme focusses on changes in atmospheric demand that are associated with increasing temperatures

* Corresponding author.
E-mail address: sewolf@ethz.ch (S. Wolf).

http://dx.doi.org/10.1016/j.jhydrol.2017.07.015
0022-1694/

as warmer air can contain more water vapour. This theme relates to the co-occurrence of dry conditions with warmer temperatures during specific anomalous events (such as 2013–2014 in California) and as a consequence of anthropogenic warming from increasing atmospheric CO_2 concentrations (Diffenbaugh et al., 2015; Williams et al., 2015). The focus is to relate increases in temperature to potential evapotranspiration (PET), for instance by using drought metrics such as the Palmer Drought Severity Index (PDSI). Accordingly, it has been suggested that anthropogenic warming will increase land surface drying globally (Dai, 2013), although robust changes in dryness have not been detected for most of the global land area (Greve et al., 2014) and are likely overestimated because of simplifications in the original calculation of the PDSI (Sheffield et al., 2012; Trenberth et al., 2014). In particular, the simplified model for potential evapotranspiration used in the original PDSI only responds to changes in temperature and does not consider changes in available radiant energy, humidity and wind speed (Sheffield et al., 2012).

Increasing temperature from anthropogenic warming has been suggested to have enhanced the recent Californian drought by increasing PET as calculated using the physically based Penman-Monteith formulation (Williams et al., 2015). This is apparently consistent with other research using PET-based approaches that project increased drying over California during the 21st century, also largely because of increasing temperature that causes increasing evapotranspiration (Ault et al., 2016; Cook et al., 2015). There are two key scientific questions arising from this previous work.

First, the PET-based methods use climate model output, but they do not make the same projections as climate models because the PET-based methods use different underlying assumptions. The PET-based methods currently in use implicitly assume that increasing atmospheric CO_2 concentrations play no direct role in controlling the actual evapotranspiration from a wet vegetated surface (i.e., by setting a constant surface resistance) and are thus biased towards drying (Roderick et al., 2015). However, over wet vegetated surfaces we expect that rising CO_2 concentrations will increase the surface resistance due to a biological response of vegetation to CO_2 (Roderick et al., 2015). Indeed, comprehensive climate models do account for the increased resistance due to the biological effects of CO_2 over wet vegetated surfaces (Milly and Dunne, 2016; Swann et al., 2016). As a consequence, any PET-based method that specifies a constant surface resistance for a wet vegetated surface will generally project a drier future compared to the output from climate models (Milly and Dunne, 2016; Roderick et al., 2015; Swann et al., 2016).

Second, the above-noted PET-based methods do not distinguish the reason for a change in temperature. For example, the temperature increase observed during drought and the projected temperature increase due to the ongoing accumulation of atmospheric greenhouse gases are both implicitly assumed to be caused by the same forcing. However, this is problematic as some of the temperature increase during meteorological drought (i.e., reduced precipitation) is the result of land-surface feedbacks from reduced evaporative cooling and increased incoming solar radiation from reduced cloud cover (Yin et al., 2014). In contrast, the temperature increase due to greenhouse forcing is projected to be the result of increased incoming longwave radiation (Arrhenius, 1896) and climate model projections are consistent with that expectation (Roderick et al., 2014). Accordingly, the cause of the temperature increase during a short-term drought is not the same as that due to long-term anthropogenic forcing, and the hydrological, agricultural and ecological consequences are unlikely to be the same.

A key scientific question related to the observed temperature increases during the current Californian drought is what part is due to long-term anthropogenic warming, what part is due to dynamical circulation change (i.e., synoptic-scale atmospheric transport), what part is due to reduced precipitation and cloud cover, and what part of the temperature increase is due to land surface feedbacks from the drought itself. These confounding effects are complex and cannot be disentangled based on direct observations. Here we contribute to this scientific challenge by investigating an approach to determine the 'cause' of the warming during meteorological drought. We examine the observed anomalies in the surface energy balance during the short-term drought and compare those with the changes expected because of long-term anthropogenic forcing. This study focuses on the biosphere-atmosphere interactions and does not attempt to investigate the important question of whether long-term anthropogenic forcing causes short-term perturbations in atmospheric circulation dynamics that are associated with meteorological drought.

In this study, we use the radiative signature concept (Yin et al., 2014) to investigate the cause of the warming associated with the 2013–2014 drought in California compared to the period 2001–2012. Note that our study investigates the cause of temperature changes during the recent drought while excluding potential long-term impacts of anthropogenic warming on drought. We use the CMIP5 model ensemble to characterise changes in the surface energy balance associated with long-term anthropogenic forcing. For the recent drought, we first examine the relation between precipitation and near-surface air temperature to confirm the widely reported negative correlation during drought. We then use observations from the CERES (NASA) satellite-derived surface radiation database to examine the state-wide radiative signature of the recent drought and contrast those results with the radiative signature of warming projected to occur by the end of the 21st century. We complement the state-wide results using direct measurements of the heat and mass fluxes from a long-term flux tower at the Vaira Ranch site located in Central California. We further extend the radiative signature approach by investigating surface feedbacks (i.e., changes in net radiation and the partitioning between latent and sensible heat flux) during the drought at the flux tower site, and also use satellite remote sensing estimates from MODIS for the latent heat flux to investigate surface feedbacks across the entire state. The objectives of this study are to: (i) use radiative signatures to quantify short-term perturbations in the surface energy balance during the Californian drought of 2013–2014; (ii) quantify the relative contributions of these perturbations and land-surface feedbacks to the observed warming; and (iii) to compare the observed surface energy balance perturbations during drought to perturbations in the surface energy balance caused by long-term anthropogenic forcing.

2. Data and methods

2.1. Study area

The study area (Fig. 1)[1] covers three nested levels: (i) the entire state of California (CA); (ii) the key agricultural region known as the Central Valley (CV); and (iii) a flux tower site at Vaira Ranch. To account for the distinct Mediterranean climate of California, all analyses used a monthly basis with separate totals calculated for the wet (Oct–Apr) and dry (May–Sep) periods and for the water year (WY, Oct–Sep). We compared the surface energy balance terms for water years in 2013 and 2014 relative to the decadal mean of 2001–2012 for the state-wide analysis but used a shorter period (2004–2012) because of reduced data availability for the fluxes measured at the Vaira Ranch flux tower.

[1] For interpretation of colour in Figs. 1 to 7, the reader is referred to the web version of this article.

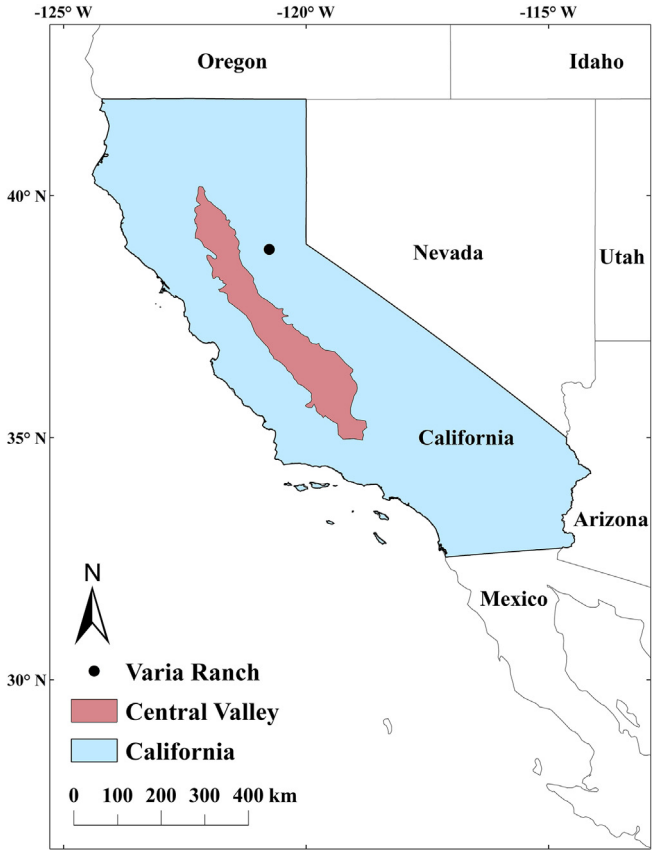

Fig. 1. Location of the study areas California (CA), the Central Valley (CV) and the AmeriFlux eddy covariance tower site at Vaira Ranch.

2.2. Climate and satellite data

Near surface air temperature (T, in °C) and precipitation (P, in mm) were extracted from the PRISM (Parameter elevation Regression on Independent Slopes Model, http://www.prism.oregonstate.edu) statistical mapping system (Daly et al., 2002) at 4 km (0.04°) spatial resolution from 1895–2014. In addition, we used two additional databases to verify that the conclusions of the study were independent of the P and T data source. The Climate Research Unit (CRU) of the University of East Anglia database (Harris et al., 2014) (version CRU TS3.22) and the U.S. Climate Divisional Dataset (Vose et al., 2014) (http://www.ncdc.noaa.gov/cag; thereafter referred to as NOAA-NCEI) were used as comparison to PRISM across California in the Supporting Information (Table S1).

To establish the radiative signatures of drought (for CA, CV), we used monthly estimates of radiation fluxes from NASA's Clouds and Earth's Radiant Energy Systems (CERES) program. The CERES database (http://ceres.larc.nasa.gov) contains observation-based estimates of the four surface radiative fluxes (incoming and outgoing shortwave and longwave) at 1° spatial resolution, available since March 2000 (Loeb et al., 2012). For the latent heat flux, we used observationally constrained model estimates of actual evapotranspiration (ET, in mm) from the Moderate Resolution Imaging Spectroradiometer (MODIS) (Mu et al., 2011) provided at 1 km spatial resolution by the Numerical Terradynamic Simulation Group at the University of Montana (http://www.ntsg.umt.edu/project/mod16). Validations of the MODIS ET product across multiple flux tower sites showed that the mean uncertainties are about 24% of the ET measured at flux towers, which is within the range of uncertainties reported for ET flux tower measurements (Mu et al., 2011).

In addition, we used direct measurements of the surface energy balance from the AmeriFlux (http://ameriflux.ornl.gov) eddy-covariance site known as Vaira Ranch (38 °24′24″ N, 120 °57′3″, 129 m a.s.l., Fig. 1), located in the Sierra Nevada foothills near the Central Valley (Baldocchi and Ma, 2013; Ma et al., 2016). Ecosystem fluxes of carbon dioxide, water vapour and energy exchange along with meteorological variables (e.g. temperature, precipitation, soil moisture, soil temperature, ground heat flux) have been measured at Vaira Ranch since late 2000, and the four components of the radiative fluxes since early 2004. The half-hourly data were quality-filtered and gap-filled according to AmeriFlux standards (Boden et al., 2013), and were aggregated to monthly, seasonal and annual time-scales. The energy balance closure at Vaira Ranch was about 70% and we used the data as observed, i.e. closure was not forced for our analyses (see e.g. Foken et al., 2012).

To establish the radiative signature associated with long-term greenhouse forcing we used the Coupled Model Intercomparison Project Phase 5 (CMIP5) projections for California. We extracted the multi-model ensemble mean (one member per model, 36–39 models depending on variable) for the Representative Concentration Pathway (RCP) 8.5, which corresponds to a high greenhouse gas emissions or 'business-as-usual' scenario (Riahi et al., 2011), for near surface climate (T, P), the four (incoming and outgoing shortwave and longwave) surface radiative fluxes, the sensible heat flux (H) and actual ET using the KNMI Climate Explorer (http://climexp.knmi.nl).

2.3. Theoretical basis

The analysis uses the surface energy balance,

$$R_N = R_{Si} - R_{So} + R_{Li} - R_{Lo} = LE + H + G \quad (1)$$

where the net radiation (R_N) at the surface is equal to the sum of incoming and outgoing shortwave (R_{Si}, R_{So}) and longwave (R_{Li}, R_{Lo}) surface radiative fluxes, which are balanced by the latent (LE), sensible (H) and ground heat (G) fluxes (all in W m^{-2}). For California and the Central Valley, the four radiative fluxes (R_{Si}, R_{So}, R_{Li}, R_{Lo}) were extracted from the CERES database, and LE (W m^{-2}) was derived from the MODIS ET (mm) estimates using the latent heat of vaporization (L). We further assumed G was negligible at the monthly to annual time scale and estimated H for California and the Central Valley using energy balance ($H = R_N - LE$; all in W m^{-2}). All fluxes (including G) were directly measured at Vaira Ranch.

We refer to the IPCC-based definition of drought as abnormally dry weather, and meteorological drought as a period with abnormal precipitation deficits (IPCC, 2014). Note that drought in a statistical sense is an extreme, i.e. a deviation from the prevailing mean climatic conditions.

2.4. Selection of a suitable baseline for the short- and long-term forcing

To characterise short-term changes in the surface energy balance due to meteorological drought (2013–2014), we were restricted to a post-2001 analysis period by the start of the CERES observational radiation database. We investigated numerous alternative baselines (Tables S2–3) and found that the difference between the drought years (2013–2014) and the decadal mean 2001–2012 produced robust T and P anomalies compared to the climatological mean of 1981–2010, which represents the current climatatological mean. The underlying reason was the PRISM T data showed a slight decrease in T for California (Table S2) for the 2001–2012 period. This also held in the CRU and NOAA-NCEI databases and is consistent with reduced warming trends that were observed globally during the period 1998–2012 (Medhaug et al., 2017).

To characterise long-term changes in the surface energy balance caused by anthropogenic forcing, we use the CMIP5 ensemble and compare the projection for the years 2089–2100 with the decadal mean for 2001–2012 to establish the projected pattern of change caused by anthropogenic forcing.

3. Results

3.1. T and P anomalies during the 2013–2014 California drought

The water years (Oct-Sep) 2013 (+0.4 °C) and 2014 (+1.0 °C) were both substantially warmer across the entire state of California than the decadal mean of 15.4 ± 0.4 °C (mean ± standard deviation, 2001–2012) (Fig. 2d–f, Table 1). Accordingly, the warmer temperatures were outside the range of decadal variability during the water year 2014 (Fig. 2d). The total P anomalies were larger in 2014 (-248 mm yr^{-1}) than in 2013 (-91 mm yr^{-1}, Fig. 2a–c) and the seasonal time course showed that the P anomaly occurred earlier (about Nov–Jan) during the water year 2014 in comparison to 2013 (about Jan–Apr). The water year 2014 P anomaly was also outside the range of decadal variability (Fig. 2a, see also Table S3). The results for the Central Valley and for Vaira Ranch were both broadly similar (Fig. S1) and the results confirm the widely reported co-occurrence of warm temperatures with low precipitation totals.

3.2. Radiative signature of drought in 2013 and 2014

In terms of the radiant heating source, we report a reduction in R_{Li} in both 2013 and 2014 (Fig. 3a–c) that was more pronounced during the wet season and more or less followed the time course of the precipitation anomaly in both 2013 and 2014 (Fig. 2a–c). Changes in R_{Lo} during drought broadly followed the R_{Li} during the wet season but not during the dry season (Fig. 3g–i). For the other radiant heating source, the incoming shortwave radiation, we found a large increase in R_{Si} during drought (about +10 W m^{-2} during the wet season in both the 2013 and 2014 water years) with the seasonal course of the anomaly again roughly following the precipitation anomaly (*cf.* Figs. 2 and 3). The anomalies in R_{So} (Fig. 3j–l) more or less tracked those of R_{Si} but with a reduced amplitude (Fig. 3d–f) and we found little evidence for any change in albedo. The state-wide radiative signature during meteorological drought was for increased incoming shortwave radiation combined with decreased incoming longwave radiation (Fig. 4) that was consistent at both the Central Valley (Fig. S2) and Vaira Ranch flux tower (Fig. S3) sites.

On a state-wide basis, the increase in R_{Si} dominated over the decrease in R_{Li} and R_N was higher throughout the water years 2013 (wet: +5.2 W m^{-2}, dry: +4.0 W m^{-2}) and 2014 (wet: +5.3 W m^{-2}, dry: +6.1 W m^{-2}; Fig. 5a–c, Table 1). Hence there was an increase in the net radiation of approximately +5 W m^{-2} during the drought years relative to the period of 2001–2012 (Table 1).

3.3. Land-surface feedbacks

Despite increased available net radiant energy (about +5 W m^{-2}) during the two drought years, the MODIS based estimates for California show declines in the latent heat flux in both the 2013 (wet: -2.0 W m^{-2}, dry: -0.9 W m^{-2}) and 2014 (wet: -4.0 W m^{-2}, dry: -2.7 W m^{-2}) water years relative to the 2001–2012 decadal mean (Fig. 5a–f, Table 1). The increase in net radiation combined with the decrease in latent heat flux resulted in a large increase in the estimate of sensible heat flux throughout both the 2013 (wet: +7.2 W m^{-2}, dry: +4.9 W m^{-2}) and 2014 (wet: +9.3 W m^{-2}, dry: +8.8 W m^{-2}) water years (Fig. 5, Table 1). The results were virtually identical for the Central Valley (Fig. S4). However, at the Vaira Ranch flux site, while the decline in latent heat flux during drought was consistent with state-wide estimates, the net radiation was generally lower during the drought years leading to a much smaller increase in sensible heat flux in 2013 and little change in 2014 (Fig. S4). The smaller anomalies at Vaira are likely related to an underestimation of the measured turbulent fluxes due to a lack of energy balance closure (see Section 2.2).

In terms of the state-wide (and Central Valley) results, the estimated increase in sensible heat flux ($\Delta H = \Delta R_N - L\Delta E$) during the 2013 (=6.4 W m^{-2} = 4.8 – (−1.6) = 4.8 + 1.6) and 2014 (9.1 W m^{-2} = 5.5 – (−3.6) = 5.5 + 3.6) water years (Fig. 5g–i) was mostly (~2/3) attributable to an increase in net radiation with the remainder (~1/3) due to a reduction in latent heat flux. The increase in ΔH during drought was therefore a consequence of (1) more available energy due primarily to increased solar

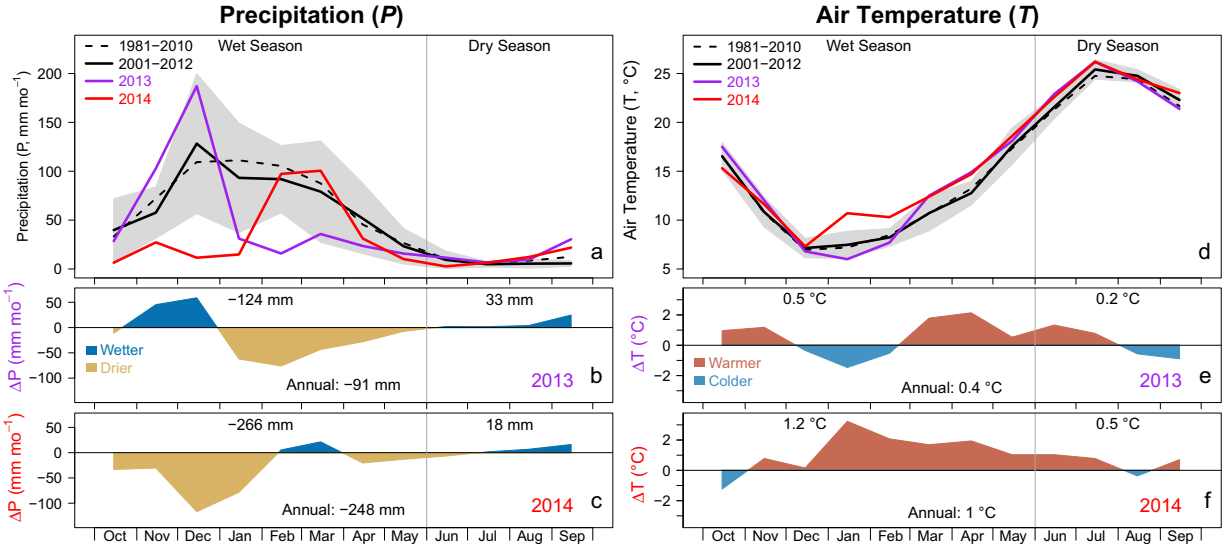

Fig. 2. Monthly (a) total precipitation (P, mm mo^{-1}) and (d) mean air temperature (T, °C) across California based on PRISM during the wet (Oct–May) and dry (Jun–Sep) seasons of the water year (Oct–Sep) in both 2013 and 2014 compared to the decadal mean for 2001–2012. Gray shading denotes the standard deviation of the decadal mean. The lower panels show the anomalies for 2013 (b, e) and 2014 (c, f) relative to the decadal mean. Numbers denote the seasonal and annual anomalies. The climatological means for 1981–2010 (a, d) are shown as dashed lines for comparison.

Table 1
Climate anomalies during the water years (WY, Oct–Sep), the wet (Oct–May) and dry (Jun–Sep) seasons of 2013 and 2014 compared to the decadal mean of 2001–2012. Unlike for California and the Central Valley, directly measured radiation fluxes for Vaira Ranch were available only since 2004 (with anomalies calculated relative to 2004–2012). Measured ground heat flux (G) was only available for Vaira Ranch and the relatively small observed anomalies (<1.1 W m^{-2}, also see Fig. S5) justify our approximation that $G \sim 0$ for California and for the Central Valley.

	California						Central Valley						Vaira Ranch					
	2013			2014			2013			2014			2013			2014		
	WY	Wet	Dry	WY	Wet	Dry	WY	Wet	Dry	WY	Wet	Dry	WY	Wet	Dry	WY	Wet	Dry
ΔP (mm)	–191	–124	+33	–248	–266	+18	–79	–182	+2	–149	–150	+1	–116	–123	+7	–155	–166	+12
ΔT (°C)	+0.4	+0.5	+0.2	+1.0	+1.2	+0.5	+0.5	+0.6	+0.2	+1.0	+1.1	+0.8	+0.7	+0.8	+0.2	+1.2	+1.3	+0.8
ΔR_{Si} (W m^{-2})	+5.0	+9.3	–3.4	+6.3	+10.5	–2.2	+8.2	+12.9	–1.2	+7.7	+13.1	–3.1	+12.5	+18.4	+0.6	+16.7	+23.9	+2.2
ΔR_{So} (W m^{-2})	+0.8	+1.3	–0.3	+0.3	+0.7	–0.6	+2.2	+2.9	+0.9	+2.8	+3.9	+0.7	–0.2	+5.1	–10.8	+4.9	+4.8	+5.1
ΔR_{Li} (W m^{-2})	–2.4	–3.7	+0.1	–1.9	–3.8	+1.9	–2.6	–4.4	+1.2	–1.2	–3.7	+3.8	–5.8	–8.0	–1.4	–6.5	–12.1	+4.8
ΔR_{Lo} (W m^{-2})	–3.0	–0.9	–7.1	–1.4	+0.7	–5.8	+0.1	–0.4	+1.1	+1.5	+2.2	+0.2	+10.7	+7.8	+16.5	+10.8	+8.5	+15.5
ΔG (W m^{-2})													+0.2	+0.3	0.0	+0.9	+1.1	+0.6
ΔR_N (W m^{-2})	+4.8	+5.2	+4.0	+5.5	+5.3	+6.1	+3.3	+5.9	–2.0	+2.2	+3.3	–0.1	–3.8	–2.4	–6.5	–5.5	–1.4	–13.6
ΔLE (W m^{-2})	–1.6	–2.0	–0.9	–3.6	–4.0	–2.7	–2.0	–2.5	–0.9	–5.9	–6.5	–4.5	–2.5	–3.2	–1.3	–4.0	–4.0	–4.0
ΔH (W m^{-2})	+6.4	+7.2	+4.9	+9.1	+9.3	+8.8	+5.2	+8.4	–1.1	+8.0	+9.9	+4.4	+2.7	+4.7	–1.1	–0.4	+1.9	–5.0

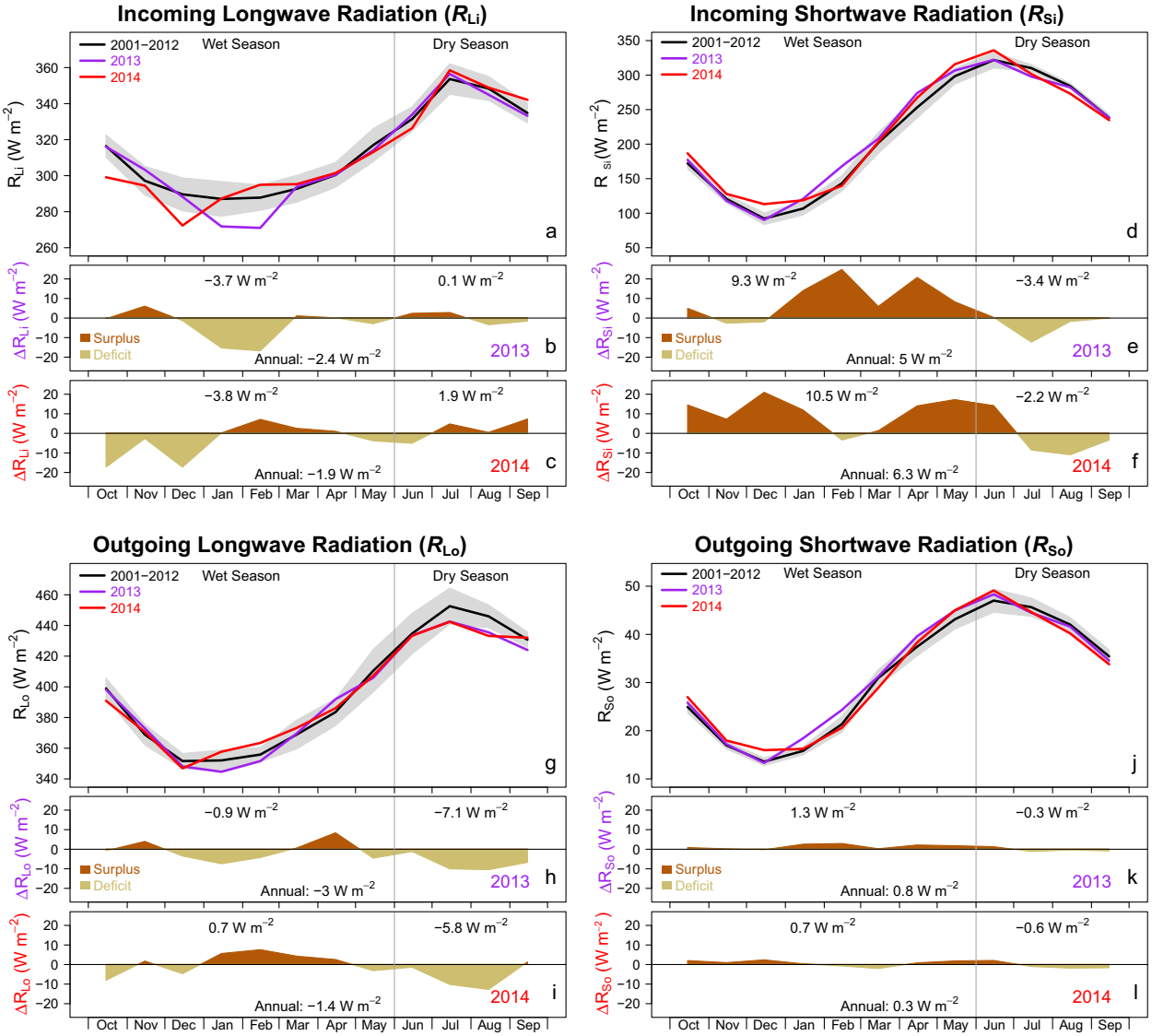

Fig. 3. Monthly mean (a) incoming longwave radiation (R_{Li}), (d) incoming shortwave radiation (R_{Si}), (g) outgoing longwave radiation (R_{Lo}) and (j) outgoing shortwave radiation (R_{So}, all in W m^{-2}) across California during the wet (Oct–May) and dry (Jun–Sep) seasons of the water year (Oct–Sep) in both 2013 and 2014 water years compared to the decadal mean of 2001–2012. Gray shading denotes the standard deviation of the decadal mean. The lower panels show the respective anomalies for 2013 (b, e, h, k) and 2014 (c, f, i, l) relative to the decadal mean. Numbers denote the seasonal and annual anomalies. Please note the different scaling of the mean (upper) panels for each radiation component while the scaling of the anomaly panels is identical throughout to enable direct comparisons.

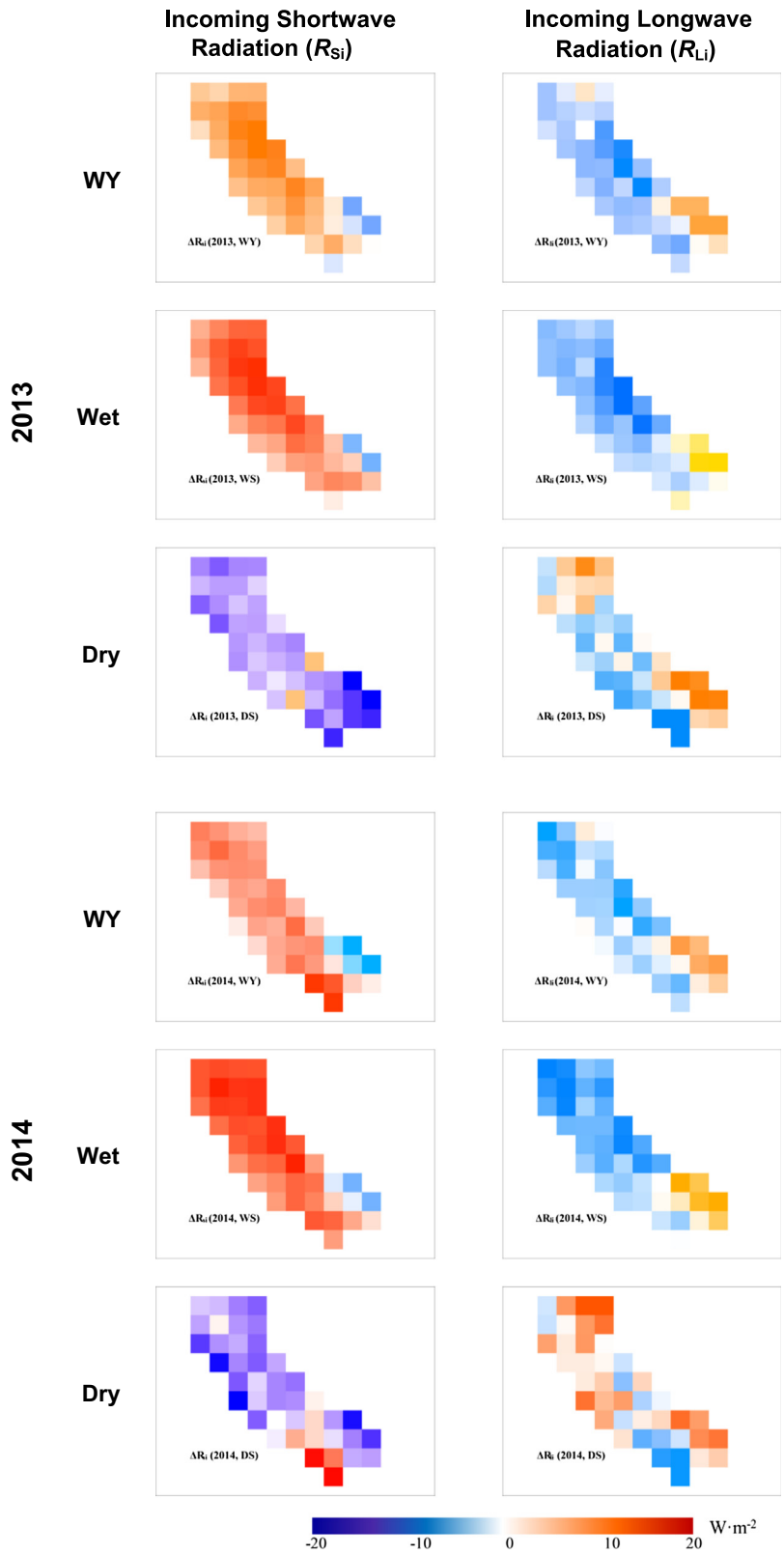

Fig. 4. Spatial anomaly maps for the incoming shortwave (R_{Si}) and longwave (R_{Li}) radiation during the wet (Oct–May) and dry (Jun–Sep) seasons of the water year (WY, Oct–Sep) in both 2013 and 2014 water years compared to the decadal mean 2001–2012 across California. See Figs. S7 and S8 for similar state-wide maps showing *P*, *T*, R_N, *LE*, *H*.

radiation and (2) of reduced latent heat flux (and thus reduced evaporative cooling) due to drought related reductions in the supply of water (i.e., precipitation) for actual *ET*. The combination of those changes both contributed to higher temperatures during the drought (Fig. 5).

3.4. Radiative signature of anthropogenic warming

The CMIP5 (RCP8.5 scenario) multi-model ensemble mean projects increases of 4.2 °C in mean water year air temperature across California by 2089–2100 relative to 2001–2012, with higher

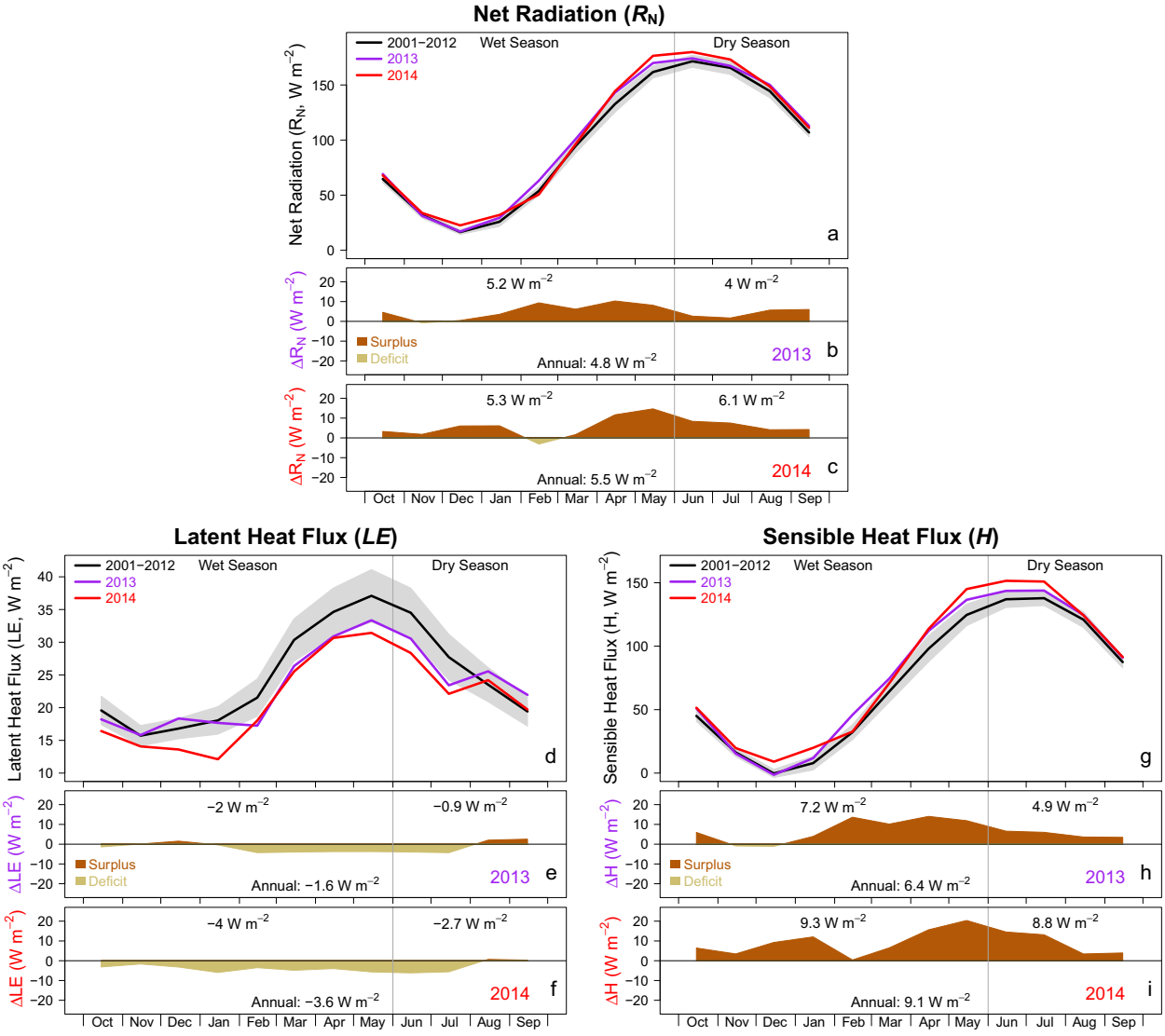

Fig. 5. Monthly (a) mean net radiation (R_N), (d) latent heat flux (*LE*) and (g) sensible heat flux (*H*, all in W m^{-2}) across California during the water years (Oct–Sep) 2013 and 2014 compared to the decadal mean of 2001–2012. Gray shading denotes the standard deviation of the decadal mean. The lower panels show the respective anomalies for 2013 (b, e, h) and 2014 (c, f, i) relative to the decadal mean. Numbers denote the seasonal and annual anomalies. Please note the different scaling of the mean (upper) panels while the scaling of the anomaly panels is identical throughout to enable direct comparisons.

increases during the dry compared to the wet season (Figs. 6a & S6, Table 2). In contrast, monthly mean precipitation is projected to remain very similar to current levels (2001–2012) with a minor increase (+14 mm yr^{-1}) projected for the wet season. The radiative signature showed a substantial increase in the incoming longwave radiation (+27.0 W m^{-2}) by the end of the 21st century that was projected to be higher during the dry (+37.6 W m^{-2}) compared to the wet season (+21.8 W m^{-2}) (Figs. 6c & 7a–b, Table 2). Only minor changes were projected for the incoming shortwave radiation over either the water year (−0.9 W m^{-2}) or in the wet (+1.6 W m^{-2}) or dry (−5.7 W m^{-2}) seasons (Figs. 6e & 7c–d). In summary, the overall trend until end of the 21st century is projected as increasing longwave radiation (incoming and outgoing, Fig. 6c–d) and minor reductions in shortwave radiation (Fig. 6e–f), with net radiation increasing at the land surface (Fig. 6g).

The observations reported here show that the radiative signature of the current Californian drought is for a large increase in incoming shortwave radiation coupled with a moderate decrease in incoming longwave radiation (Fig. 3a–f). In contrast, the radiative signature of the projected warming associated with long-term anthropogenic forcing shows little change in incoming shortwave radiation coupled with a very large increase in the incoming longwave radiation (Fig. 7, Table 2). Further, Fig. 6 highlights that the hydrological and ecological consequences of the forcing during the short-term drought are very different from those related to the long-term forcing. For example, consider first the long-term model projections. The CMIP ensemble projects warming of around 4.2 °C by the end of the 21st century. Physically, this is associated with an increase in the outgoing longwave radiation from the surface. Using the black-body sensitivity (=4 σ T^3 ~ 5.3 W m^{-2} K^{-1} at a mean T of 13 °C) suggests an increase in outgoing longwave radiation of around (4.2 × 5.3 = 22.3 W m^{-2}) which is more or less identical with the model projection of 23.4 W m^{-2} (Fig. 6e). Accordingly, the land surface warms in the model projections and the outgoing longwave radiation increases mostly because of increases in the incoming longwave radiation. However, net radiation shows little change and despite the projected warming, the CMIP5 projections

show little change for actual *ET* (Fig. 6c). The underlying physical reason is that actual *ET* is constrained by the available radiant energy (i.e. net radiation) and water supply (i.e. precipitation). In summary, the CMIP5 ensemble projections for greenhouse warming over California project large increases in *T* with little change in either *P* or actual *ET*.

4. Discussion

4.1. The radiative signature of short-term meteorological drought

Our analyses of changes in the two incoming radiative fluxes have revealed a radiative signature of increased incoming short-

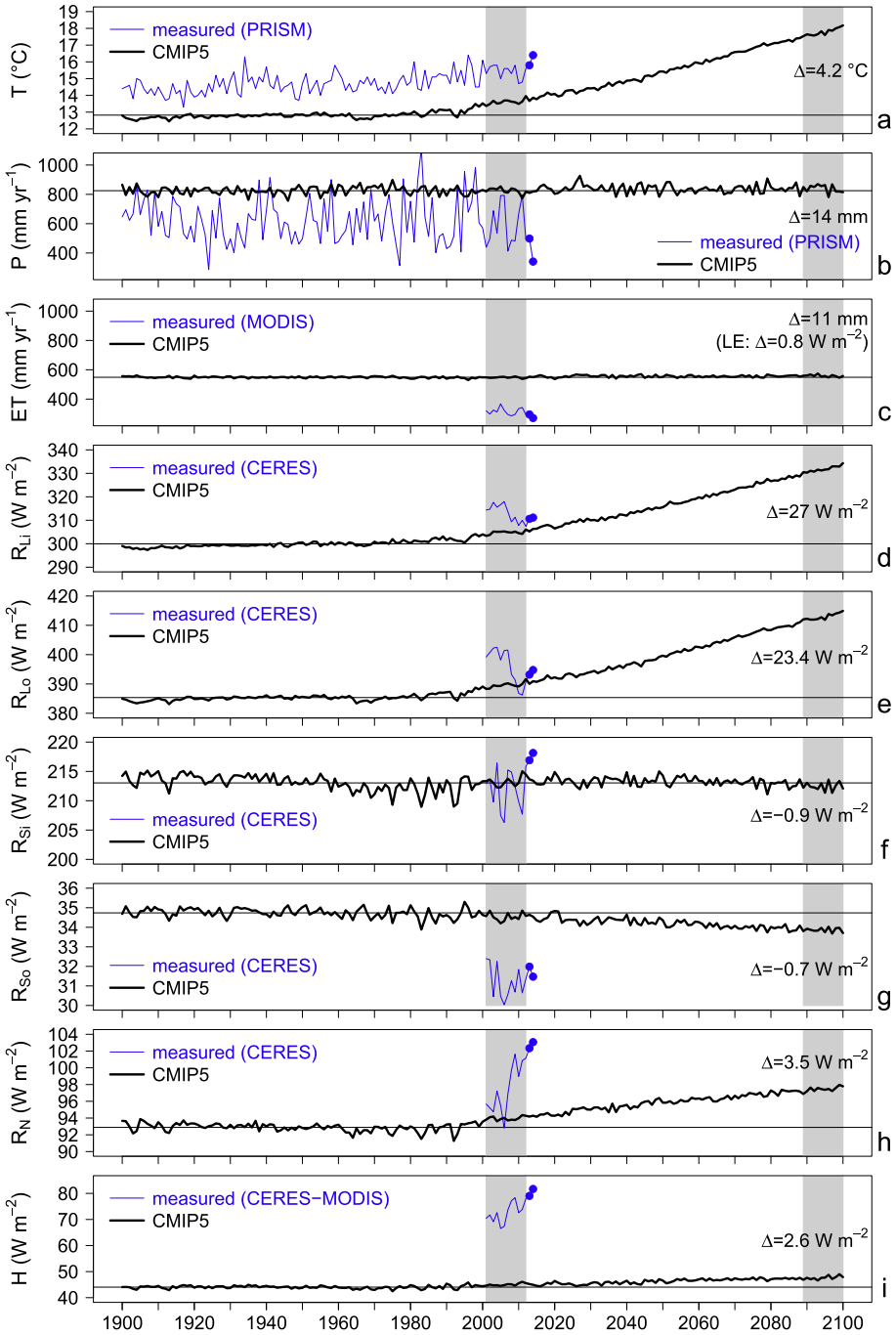

Fig. 6. Long-term time series of (a) mean near surface air temperature (*T*), (b) total precipitation (*P*), (c) total actual evapotranspiration (*ET*), (d) mean longwave incoming (R_{Li}), (e) mean longwave outgoing (R_{Lo}) and (f) shortwave incoming radiation (R_{Si}), (g) mean shortwave outgoing (R_{So}), (h) mean net radiation (R_N) and (i) sensible heat flux (*H*) for the water years (Oct.-Sep.) from 1900 to 2100 across California based on CMIP5 multi-model mean (RCP8.5 scenario). Grey shadings highlight the decades 2001–2012 and 2089–2100, which are used for seasonal radiative signatures in Fig. 7. Blue lines denote measured data from meteorological stations (for *T* and *P* from PRISM, 1900–2014), MODIS (for *ET*, 2001–2014) and CERES observations (for R_{Li}, R_{Lo}, R_{Si}, R_{So}, R_N, 2001–2014), blue dots mark the years 2013 and 2014. Numbers denote the mean water year anomaly for the decade 2089–2100 compared to 2001–2012. For *ET* the anomaly is also converted to latent heat flux (*LE*) for comparability. The larger inter-annual variability of the observations (PRISM, MODIS, CERES) than from the ensemble projections from CMIP5 is due to model-observation bias and because the year-to-year variations in the individual CMIP5 model runs cancel out in the ensemble averaging (Sun et al., 2011).

Table 2
Climate anomalies during the water year (WY, Oct–Sep), wet (Oct–May) and dry (Jun–Sep) seasons at the end of the 21st century (decade 2089–2100) compared to the decadal mean of 2001–2012 across California based on the multi-model ensemble mean of CMIP5 climate model projections (RCP8.5 Scenario). See Table S4 for a similar comparison based on PRISM (*P*, *T*), MODIS (*LE*) and CERES observations.

	California		
	WY	Wet	Dry
ΔP (mm)	14.3	17.0	–2.7
ΔT (°C)	4.2	3.8	4.9
ΔR_{Si} (W m^{-2})	–0.9	1.6	–5.7
ΔR_{So} (W m^{-2})	–0.7	–0.6	–0.8
ΔR_{Li} (W m^{-2})	27.0	21.8	37.6
ΔR_{Lo} (W m^{-2})	23.4	20.4	29.3
ΔR_N (W m^{-2})	3.5	3.5	3.4
ΔLE (W m^{-2})	0.8	2.0	–1.6
ΔH (W m^{-2})	2.6	1.9	3.9

wave radiation coupled with reductions in the incoming longwave radiation (both presumably due to reduced water vapour and/or cloud cover) during the Californian drought 2013–2014 relative to the earlier 2001–2012 decade (Fig. 3a–f, Table 1). This pattern is identical with that shown previously for four other regions worldwide during meteorological drought (Yin et al., 2014). A closer examination of the results showed that the seasonal time course for increased incoming shortwave and decreased incoming longwave during 2013–2014 (Fig. 3a–f) more or less followed the seasonal perturbation in precipitation (Fig. 2a–c). That the radiation and precipitation should track together is no real surprise because we intuitively expect meteorological drought to be associated with reduced cloud cover. This in turn results in increased incoming shortwave but reduced incoming longwave radiation. Here we found the increase in shortwave dominated over the decrease in longwave and there was an increase in net radiation throughout much of the 2013 and 2014 water years of about +5 W m^{-2} during the drought, compared to 2001–2012 (Fig. 5a–c).

This pattern of warmer *T* during meteorological drought is common in California and occurred previously, e.g. during the droughts in 1931, 1934 and 1959. However, it is not universal as different causes of changes in *T* have different consequences. For example, the extremely low *P* during the 1976–1977 drought in California (see Fig. 6) was not obviously associated with anomalously warmer temperatures. The causation during this particular event remains unknown, yet might have been related to global dimming linked to increasing sulphur emissions from 1950–1980, which reached its peak around 1980 and was reported to have reduced R_{Si} by about ~6 W m^{-2} across the US (Wild, 2012).

4.2. Contribution of drought-induced surface feedbacks to warming

Both the increased radiant (shortwave) energy and the reduction in latent heat flux (and thereby reduced evaporative cooling) shift the partitioning of the net radiation towards the sensible heat flux. The estimated increase in sensible heat flux was mostly (~2/3) attributable to an increase in net radiation with the remaining (~1/3) being due to reduced evaporative cooling because of the lack of available water (Fig. 5d–f, Table 1). Such land-surface feedbacks have important implications for understanding local-scale temperature dynamics. For example, irrigation enhances evaporative cooling and leads to lower temperatures as is well known in the Central Valley (Christy et al., 2006; Lobell and Bonfils, 2008). While the extent of irrigated area has stabilized in California since 1980 (Bonfils and Lobell, 2007), the recent multi-year drought prompted unprecedented state-wide water restrictions in early 2014 (Seager et al., 2015; Swain et al., 2014), which reduced the farmed and irrigated area across the Central Valley (AghaKouchak et al., 2015; Cooley et al., 2015). Our analyses for the Central Valley showed direct evidence for the impact of reduced irrigation on the energy flux partitioning during 2014. In particular, with similar net radiation in 2014 compared to 2013, particularly during the dry summer season (Fig. S4, Table 1), the latent heat flux was further reduced in 2014 relative to 2013, consistent with a reduction in irrigation. Further research is needed to better quantify the effects of irrigation on regional temperatures and the associated long-term impact of groundwater depletion in the Central Valley.

4.3. The radiative signature of long-term anthropogenic forcing

Climate models project that long-term greenhouse forcing will lead to increasing near-surface air temperatures (Fig. 6a). During drought we also commonly observe a short-term (days to months to a few years) increase in air temperature. It is only natural to equate the elevated temperature during drought with future warming. However, such comparisons are only valid if the

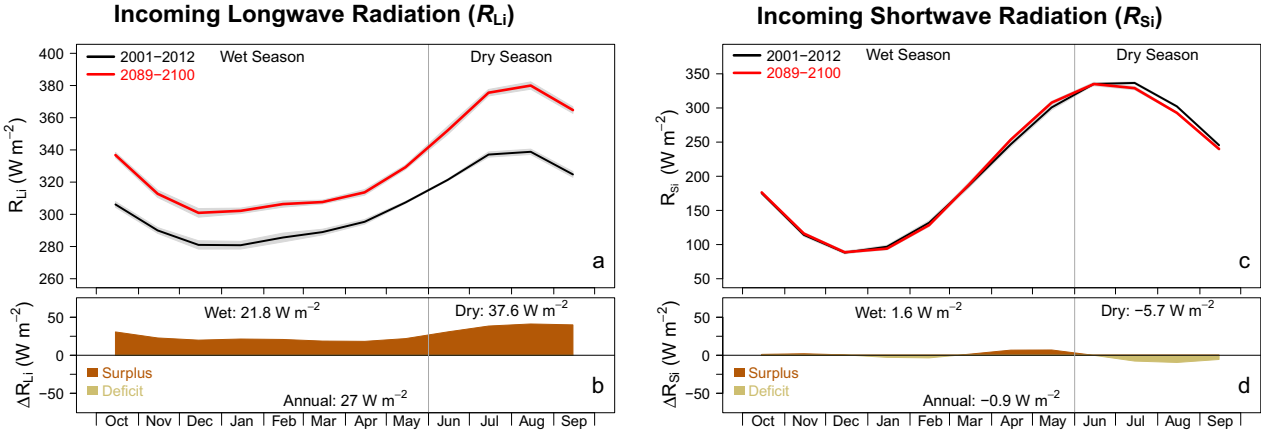

Fig. 7. Radiative signatures of anthropogenic greenhouse warming for (a) mean monthly incoming longwave (R_{Li}) and (c) shortwave (R_{Si}, both in W m^{-2}) radiation at the end of the 21st century (decade 2089–2100) compared to 2001–2012 across California based on multi-model mean CMIP5 multi-model mean (RCP8.5 scenario). The lower panels (b, d) show the respective anomalies in 2089–2100 compared to the decadal mean of 2001–2012. Numbers denote the seasonal and annual anomalies. The Supporting Information (Tables S6–7) also shows the years 2013–2014 and baseline period 2001–2012 compared to the early last century (1901–1912), and other variables projected from CMIP5 across California (Fig. S6).

underlying physical basis for the warming is the same. For example, the warming that current climate models project to result from enhanced greenhouse forcing over the coming century is due to a relatively small direct effect of atmospheric CO_2 that is amplified by a positive water vapour feedback (Held and Soden, 2000) that together result in a large (projected) increase in incoming longwave radiation with little change in shortwave radiation (Roderick et al., 2014). Hence the primary physical signal for the temperature increase associated with long-term anthropogenic forcing is for increased incoming longwave radiation (Figs. 6c & 7a–b, Table 2) and increased mean specific atmospheric humidity. In contrast, during a short-term meteorological drought, such as the 2013–2014 Californian drought, the atmospheric CO_2 continues to accumulate but the direct radiative effect is only small over the two years. For example, current observations put the increase in incoming longwave radiation due to the direct radiative effect of CO_2 at around 0.02 W m^{-2} yr^{-1} (Feldman et al., 2015). Over the two year period considered here (2013–2014), that change is around two orders of magnitude smaller than the observed perturbations in other surface energy balance terms (Figs. 3–5, Table 1). Of course, the long-term warming due to atmospheric CO_2 is projected to be amplified by a positive water vapour feedback (Held and Soden, 2000). However, during a meteorological drought, we can reasonably expect a negative water vapour feedback that would be consistent with the reduction in incoming longwave radiation (Fig. 3a–c, Table 1). Both drought-induced and greenhouse-induced warming are the result of more incoming radiant energy at the land surface. The key point is that the underlying physical cause (shortwave vs. longwave) of increases in air temperature is distinctively different during meteorological drought when compared to projections of enhanced greenhouse forcing. That is critical because different underlying causes have different consequences for the water and energy balance (Fig. 6).

By extending the concept of Yin et al. (2014), our analyses demonstrate that radiative signatures are a powerful tool to differentiate drought-induced warming from greenhouse-induced warming at monthly to seasonal to interannual time scales. Drought-induced warming is associated with increased incoming shortwave radiation and a decrease in the incoming longwave while greenhouse-induced warming is characterized by increased incoming longwave radiation. Future studies can employ this approach to systematically assess droughts at regional, continental and global scales.

4.4. The cause and intensity of the Californian drought

The radiative signature concept has been used here to infer that increased air temperature during the Californian drought was largely the result of increased incoming shortwave radiation. However, our analysis does not, and cannot: (i) quantify the impact of anthropogenic warming on drought, and cannot; (ii) attribute the dynamical cause of the rainfall perturbation. In particular, the recent Californian drought has been associated with a synoptic blocking pattern called the 'Ridiculously Resilient Ridge', a persistent and strong midtropospheric high pressure ridge over the northeastern Pacific that displaced storm tracks northwards (Seager et al., 2015; Swain, 2015). This anomalous ridge reduced precipitation and cloud cover over California during the wet season, which in turn increased solar radiation and the available energy at the surface. The blocking also enhanced the land-atmosphere coupling from soil water limitations whereby reduced actual *ET* (and thus reduced evaporative cooling) shifted the partitioning of available net radiation towards the sensible heat flux. The cascading set of transient changes contributed both to warmer temperatures at the surface and in the adjacent atmosphere.

Initial analysis of model simulations suggested that the intensity of this anomalous ridge may have a traceable, although indirect link to anthropogenic warming via climate oscillations in the Pacific (Wang et al., 2014). Other research indicates changes of atmospheric circulation patterns linked with seasonal precipitation and temperature anomalies in California (Swain et al., 2016). However, there is also some evidence that the precipitation deficits during the Californian drought may have been dominated by natural variability (Mao et al., 2015; Seager et al., 2015) and not by rising greenhouse gases and related long-term changes in climate (Cheng et al., 2016). In short, the atmospheric dynamics that underlie variations in precipitation (and hence meteorological drought) remain a topic of ongoing research.

5. Conclusion

We conclude that much of the warming associated with the 2013–2014 Californian drought was a transient short-term perturbation caused by severe precipitation deficits, and associated with increased solar radiation (presumably due to reduced cloud cover) in combination with a land-surface feedback (reduced evaporative cooling) that further exacerbated the warming. Both drought and the enhanced greenhouse effect are associated with warmer temperatures but the underlying physical cause and associated radiative perturbations are very different. The consequences for water availability are also very different. The radiative signature of this Californian drought clearly showed increasing incoming shortwave (i.e., solar) radiation coupled with a decline in incoming longwave radiation. In contrast, global warming projections (for California and elsewhere) show increased temperature as a consequence of the elevated greenhouse effect from increased incoming longwave radiation. Distinguishing the source of the radiative perturbation is a new approach that can be used as a basis for attributing the cause of warming during drought.

Acknowledgements

This research was supported by the European Commission's FP7 (S.W., Marie Curie International Outgoing Fellowship, grant 300083) and ETH Zurich. D.Y and M.L.R are supported by the Australian Research Council (CE11E0098), and D.Y. acknowledges support by the National Natural Science Foundation of China (51609122). We gratefully acknowledge Siyan Ma and Dennis Baldocchi for providing flux tower data from the AmeriFlux site Vaira Ranch. We thank Eugenie Paul-Limoges, Guillermo Murray-Tortarolo, the editors and three anonymous reviewers for helpful comments on earlier versions of the manuscript. All data used in this paper are available online as referenced in the 'Data and Methods' section.

Appendix A. Supplementary Information

Supplementary data associated with this article can be found, in the online version, at http://dx.doi.org/10.1016/j.jhydrol.2017.07.015.

References

AghaKouchak, A., Feldman, D., Hoerling, M., Huxman, T., Lund, J., 2015. Recognize anthropogenic drought. Nature 524 (7566), 409–411.

Arrhenius, S., 1896. On the influence of carbonic acid in the air upon the temperature of the ground. Philos. Mag. J. Sci. 41 (251), 237–276. http://dx.doi.org/10.1080/14786449608620846.

Ault, T.R., Mankin, J.S., Cook, B.I., Smerdon, J.E., 2016. Relative impacts of mitigation, temperature, and precipitation on 21st-century megadrought risk in the American Southwest. Sci. Adv. 2 (10). http://dx.doi.org/10.1126/sciadv.1600873.

Baldocchi, D., Ma, S., 2013. How will land use affect air temperature in the surface boundary layer? Lessons learned from a comparative study on the energy balance of an oak savanna and annual grassland in California, USA. Tellus B 65, 19994. http://dx.doi.org/10.3402/tellusb.v65i0.19994.

Boden, T.A., Krassovski, M., Yang, B., 2013. The AmeriFlux data activity and data system: an evolving collection of data management techniques, tools, products and services. Geosci. Instrum. Method Data Syst. 2 (1), 165–176. http://dx.doi.org/10.5194/gi-2-165-2013.

Bonfils, C., Lobell, D., 2007. Empirical evidence for a recent slowdown in irrigation-induced cooling. Proc. Natl. Acad. Sci. 104 (34), 13582–13587. http://dx.doi.org/10.1073/pnas.0700144104.

Cheng, L. et al., 2016. How has human-induced climate change affected California drought risk? J. Clim. 29 (1), 111–120. http://dx.doi.org/10.1175/JCLI-D-15-0260.1.

Christy, J.R., Norris, W.B., Redmond, K., Gallo, K.P., 2006. Methodology and results of calculating Central California surface temperature trends: evidence of human-induced climate change? J. Clim. 19 (4), 548–563. http://dx.doi.org/10.1175/JCLI3627.1.

Cook, B.I., Ault, T.R., Smerdon, J.E., 2015. Unprecedented 21st century drought risk in the American Southwest and Central Plains. Sci. Adv. 1 (1). http://dx.doi.org/10.1126/sciadv.1400082.

Cooley, H., Donnelly, K., Phurisamban, R., Subramanian, M., 2015. Impacts of California's Ongoing Drought: Agriculture. Pacific Institute, Oakland, California.

Dai, A., 2013. Increasing drought under global warming in observations and models. Nat. Clim. Change 3 (1), 52–58. http://dx.doi.org/10.1038/nclimate1633.

Daly, C., Gibson, W.P., Taylor, G.H., Johnson, G.L., Pasteris, P., 2002. A knowledge-based approach to the statistical mapping of climate. Clim. Res. 22 (2), 99–113.

Diaz, H.F., Wahl, E.R., 2015. Recent California water year precipitation deficits: a 440-year perspective. J. Clim. 28 (12), 4637–4652. http://dx.doi.org/10.1175/JCLI-D-14-00774.1.

Diffenbaugh, N.S., Swain, D.L., Touma, D., 2015. Anthropogenic warming has increased drought risk in California. Proc. Natl. Acad. Sci. 112 (13), 3931–3936. http://dx.doi.org/10.1073/pnas.1422385112.

Feldman, D.R. et al., 2015. Observational determination of surface radiative forcing by CO_2 from 2000 to 2010. Nature 519 (7543), 339–343. http://dx.doi.org/10.1038/nature14240.

Foken, T., Leuning, R., Oncley, S.R., Mauder, M., Aubinet, M., 2012. Corrections and data quality control. In: Aubinet, M., Vesala, T., Papale, D. (Eds.), Eddy Covariance. A Practical Guide to Measurement and Data Analysis. Springer, Netherlands, Dordrecht, pp. 85–131. http://dx.doi.org/10.1007/978-94-007-2351-1_4.

Greve, P. et al., 2014. Global assessment of trends in wetting and drying over land. Nat. Geosci. 7 (10), 716–721. http://dx.doi.org/10.1038/ngeo2247.

Griffin, D., Anchukaitis, K.J., 2014. How unusual is the 2012–2014 California drought? Geophys. Res. Lett. 41 (24). http://dx.doi.org/10.1002/2014GL062433. 2014GL062433.

Harris, I., Jones, P.D., Osborn, T.J., Lister, D.H., 2014. Updated high-resolution grids of monthly climatic observations – the CRU TS3.10 dataset. Int. J. Climatol. 34 (3), 623–642. http://dx.doi.org/10.1002/joc.3711.

Held, I.M., Soden, B.J., 2000. Water vapor feedback and global warming. Annu. Rev. Energy Env. 25 (1), 441–475. http://dx.doi.org/10.1146/annurev.energy.25.1.441.

Howitt, R.E., Medellin-Azura, J., MacEwan, D., Lund, J.R., Sumner, D.A., 2014. Economic Analysis of the 2014 Drought for California Agriculture. Center for Watershed Sciences, University of California, Davis, California, p. 20.

IPCC, 2014. Annex II: Glossary [Mach, K.J., S. Planton and C. von Stechow (eds.)]. In: Core Writing Team, R.K. Pachauri, L.A. Meyer (Eds.), Climate Change 2014: Synthesis Report. Contribution of Working Groups I, II and III to the Fifth Assessment Report of the Intergovernmental Panel on Climate Change, IPCC, Geneva, Switzerland, pp. 117–130.

Lobell, D.B., Bonfils, C., 2008. The effect of irrigation on regional temperatures: a spatial and temporal analysis of trends in California, 1934–2002. J. Clim. 21 (10), 2063–2071. http://dx.doi.org/10.1175/2007JCLI1755.1.

Loeb, N.G. et al., 2012. Observed changes in top-of-the-atmosphere radiation and upper-ocean heating consistent within uncertainty. Nat. Geosci. 5 (2), 110–113. http://dx.doi.org/10.1038/ngeo1375.

Ma, S., Baldocchi, D., Wolf, S., Verfaillie, J., 2016. Slow ecosystem responses conditionally regulate annual carbon balance over 15 years in Californian oak-grass savanna. Agric. For. Meteorol. 228–229, 252–264. http://dx.doi.org/10.1016/j.agrformet.2016.07.016.

Mann, M.E., Gleick, P.H., 2015. Climate change and California drought in the 21st century. Proc. Natl. Acad. Sci. 112 (13), 3858–3859. http://dx.doi.org/10.1073/pnas.1503667112.

Mao, Y., Nijssen, B., Lettenmaier, D.P., 2015. Is climate change implicated in the 2013–2014 California drought? A hydrologic perspective. Geophys. Res. Lett. 42 (8), 2805–2813. http://dx.doi.org/10.1002/2015GL063456.

Medhaug, I., Stolpe, M.B., Fischer, E.M., Knutti, R., 2017. Reconciling controversies about the 'global warming hiatus'. Nature 545 (7652), 41–47. http://dx.doi.org/10.1038/nature22315.

Milly, P.C.D., Dunne, K.A., 2016. Potential evapotranspiration and continental drying. Nat. Clim. Change 6 (10), 946–949. http://dx.doi.org/10.1038/nclimate3046.

Mu, Q., Zhao, M., Running, S.W., 2011. Improvements to a MODIS global terrestrial evapotranspiration algorithm. Remote Sens. Environ. 115 (8), 1781–1800. http://dx.doi.org/10.1016/j.rse.2011.02.019.

NOAA, 2016. Climate Monitoring – Climatological Rankings, http://www.ncdc.noaa.gov/temp-and-precip/climatological-rankings.

Riahi, K. et al., 2011. RCP 8.5—A scenario of comparatively high greenhouse gas emissions. Clim. Change 109 (1), 33. http://dx.doi.org/10.1007/s10584-011-0149-y.

Roderick, M.L., Greve, P., Farquhar, G.D., 2015. On the assessment of aridity with changes in atmospheric CO_2. Water Resour. Res. 51 (7), 5450–5463. http://dx.doi.org/10.1002/2015WR017031.

Roderick, M.L., Sun, F., Lim, W.H., Farquhar, G.D., 2014. A general framework for understanding the response of the water cycle to global warming over land and ocean. Hydrol. Earth Syst. Sci. 18 (5), 1575–1589. http://dx.doi.org/10.5194/hess-18-1575-2014.

Seager, R. et al., 2015. Causes of the 2011–14 California drought. J. Clim. 28 (18), 6997–7024. http://dx.doi.org/10.1175/JCLI-D-14-00860.1.

Sheffield, J., Wood, E.F., Roderick, M.L., 2012. Little change in global drought over the past 60 years. Nature 491 (7424), 435–438. http://dx.doi.org/10.1038/nature11575.

Sun, F., Roderick, M.L., Lim, W.H., Farquhar, G.D., 2011. Hydroclimatic projections for the Murray-Darling Basin based on an ensemble derived from Intergovernmental Panel on Climate Change AR4 climate models. Water Resour. Res. 47 (12). http://dx.doi.org/10.1029/2010WR009829. W00G02.

Swain, D.L., 2015. A tale of two California droughts: Lessons amidst record warmth and dryness in a region of complex physical and human geography. Geophys. Res. Lett. 42 (22), 9999–10,003. http://dx.doi.org/10.1002/2015GL066628.

Swain, D.L., Horton, D.E., Singh, D., Diffenbaugh, N.S., 2016. Trends in atmospheric patterns conducive to seasonal precipitation and temperature extremes in California. Sci. Adv. 2 (4). http://dx.doi.org/10.1126/sciadv.1501344.

Swain, D.L. et al., 2014. The extraordinary California drought of 2013/2014: character, context, and the role of climate change. Bull. Am. Meteorol. Soc. 95 (9), S3–S7.

Swann, A.L.S., Hoffman, F.M., Koven, C.D., Randerson, J.T., 2016. Plant responses to increasing CO_2 reduce estimates of climate impacts on drought severity. Proc. Natl. Acad. Sci. 113 (36), 10019–10024. http://dx.doi.org/10.1073/pnas.1604581113.

Trenberth, K.E. et al., 2014. Global warming and changes in drought. Nat. Clim. Change 4 (1), 17–22. http://dx.doi.org/10.1038/nclimate2067.

Vose, R.S. et al., 2014. Improved historical temperature and precipitation time series for U.S. climate divisions. J. Appl. Meteorol. Climatol. 53 (5), 1232–1251. http://dx.doi.org/10.1175/jamc-d-13-0248.1.

Wang, S.Y., Hipps, L., Gillies, R.R., Yoon, J.-H., 2014. Probable causes of the abnormal ridge accompanying the 2013–2014 California drought: ENSO precursor and anthropogenic warming footprint. Geophys. Res. Lett. 41 (9), 3220–3226. http://dx.doi.org/10.1002/2014GL059748.

Wild, M., 2012. Enlightening global dimming and brightening. Bull. Am. Meteorol. Soc. 93 (1), 27–37. http://dx.doi.org/10.1175/bams-d-11-00074.1.

Williams, A.P. et al., 2015. Contribution of anthropogenic warming to California drought during 2012–2014. Geophys. Res. Lett. 42 (16), 6819–6828. http://dx.doi.org/10.1002/2015GL064924.

Yin, D., Roderick, M.L., Leech, G., Sun, F., Huang, Y., 2014. The contribution of reduction in evaporative cooling to higher surface air temperatures during drought. Geophys. Res. Lett. 41 (22), 7891–7897. http://dx.doi.org/10.1002/2014GL062039.